Acta Mech 210, 315–330 (2010)
DOI 10.1007/s00707-009-0208-x

H. N. Wang · G. H. Nie

Analytical expressions for stress and displacement fields in viscoelastic axisymmetric plane problem involving time-dependent boundary regions

Received: 2 March 2009 / Revised: 2 July 2009 / Published online: 11 August 2009

Abstract An analytical solution is developed in this paper for viscoelastic axisymmetric plane problems under stress or displacement boundary condition involving time-dependent boundary regions using the Laplace transform. The explicit expressions are given for the radial and circumferential stresses under stress boundary condition and the radial displacement under displacement boundary condition. The results indicate that the two in-plane stress components and the displacement under corresponding boundary conditions have no relation with material constants. The general form of solutions for the remaining displacement or stress field is expressed by the inverse Laplace transform concerning two relaxation moduli. As an application to deep excavation of a circular tunnel or finite void growth, explicit solutions for the analysis of a deforming circular hole in both infinite and finite planes are given taking into account the rheological characteristics of the rock mass characterized by a Boltzmann or Maxwell viscoelastic model. Numerical examples are given to illustrate the displacement and stress response. The method proposed in this paper can be used for analysis of earth excavation and finite void growth.

1 Introduction

The general static and dynamic problems are restricted to fixed boundaries, which are time-independent. However, in some practical engineering applications, such as excavation of underground tunnels, it is impossible to excavate full-section in one time. The excavation is a time-consuming procedure, during which new working face is formed constantly and variations in time and space will occur periodically. For the effect of long-period geological action, some kinds of rock (e.g. soft rock) have low strength, open grain, or contain large quantities of clay minerals. The behavior of soft rock is, in general, time-dependent or rheologic. Since the excavation is continuous, the deformation of rock material is induced due to the synthetic action of excavation and rheology. Analysis of the excavation of the soft rock is of great importance for a better understanding of excavation mechanism. The rock can be considered a viscoelastic material, and such analysis should be conducted by seeking a solution for a corresponding viscoelastic problem with time-dependent boundary region.

For various viscoelastic materials, e.g., metals and polymers, there have been numerous studies on linear and non-linear theories and applications [1–15]. Many problems of linear viscoelasticity can be solved using the principle of correspondence [16–18]. The integral-transform method and finite element method have been commonly used to solve some simple problems [19,20]. For the case of time-dependent boundary, in general, the principle is inapplicable. Specifically, for the analysis of tunnel excavation, numerical simulation is generally adopted to determine stress and displacement states during excavation, in which the continuous excavation process is divided into several steps. Considering that the corresponding rock block for each step is excavated at once at its beginning, if the step is small enough, the discrete analysis can be used effectively to simulate

H. N. Wang (✉) · G. H. Nie
School of Aerospace Engineering and Applied Mechanics, Tongji University, 200092 Shanghai, People's Republic of China
E-mail: wanghn@tongji.edu.cn

the continuous excavation in a permissible error. A corresponding finite element model was thus developed for the analysis of a foundation ditch by Mana [21]. A solution for stresses of a wedge caused by gravity was presented by Rashba [22]. This is an early analytical study on geometry time-varying problem. Analyses for stress and strain in culvert with continuous fill have been carried out, e.g. in [23,24]. Stress and strain state of a rigid inclined plane with continuous snow retention was obtained by Brown [25]. Solutions for some special problems are also addressed by Namov [26]. Recently, Shamina has simplified time-varying equations for an axisymmetric problem [27]. The dependence of compatibility equations for time-varying mechanics has been analyzed by Georgiyevskii [28]. More recently, some efforts have been made to search for solutions for viscoelastic problems involving time-dependent boundary regions using the principle of correspondence for some special cases [29–31].

Different from the purely elastic materials with constitutive equations in the form of algebraic equations, viscoelastic materials have their constitutive relations expressed by a set of operator equations. Generally, it becomes difficult to find analytical solutions for most viscoelastic problems, especially for the case of time-dependent boundary. This paper is devoted to analytical determinations on the stress and displacement fields for axisymmetric plane deformation involving time-dependent boundary regions. As an application to deep excavation of a circular tunnel or (cylindrical) void growth, explicit solutions for the analysis of a deforming circular hole in an infinite or finite plane are given taking into account the rheological characteristics of the rock mass characterized by Boltzmann and/or Maxwell viscoelastic models. Numerical examples for a circular hole subject to axisymmetric time-dependent stress or displacement are given to illustrate the displacement and stress for excavation or finite void growth.

2 Mathematical formulation

Consider a homogeneous, isotropic, and linear viscoelastic material occupying an annular region with the changeable inner and outer radii of $R_1(t)$ and $R_2(t)$, respectively, with time t, as shown in Fig. 1. For the case of axisymmetric deformation under the plane strain condition, the equilibrium equation in a cylindrical coordinate system (r, θ, z) is written

$$\frac{\partial \sigma_r(r,t)}{\partial r} + \frac{\sigma_r(r,t) - \sigma_\theta(r,t)}{r} = 0. \tag{1}$$

The geometrical equations are

$$\varepsilon_r = \frac{\partial u_r(r,t)}{\partial r}, \quad \varepsilon_\theta = \frac{u_r(r,t)}{r}, \quad \varepsilon_z = 0. \tag{2}$$

The constitutive equations can be expressed in the form of convolution integrals as

$$\begin{aligned} s_{ij}(r,t) &= 2G(t) * de_{ij}(r,t), \\ \sigma_{mm}(r,t) &= 3K(t) * d\varepsilon_{mm}(r,t). \end{aligned} \tag{3}$$

where s_{ij} and e_{ij} are the deviatoric components of the stress and strain tensors σ_{ij} and ε_{ij}, respectively, i.e.,

$$\begin{aligned} s_{ij} &= \sigma_{ij} - \frac{1}{3}\delta_{ij}\sigma_{mm}, \\ e_{ij} &= \varepsilon_{ij} - \frac{1}{3}\delta_{ij}\varepsilon_{mm}. \end{aligned} \tag{4}$$

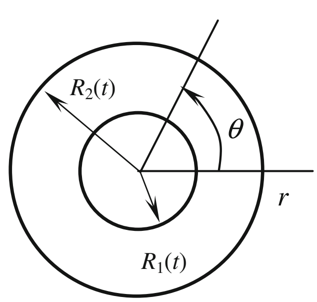

Fig. 1 Axisymmetric plane problem involving time-dependent region

and $G(t)$ and $K(t)$ are relaxation moduli incorporating viscoelastic effect of materials. The asterisk $(*)$ in Eq. (3) indicates a convolution integral defined by

$$f_1(t) * df_2(t) = f_1(t) \cdot f_2(0) + \int_0^t f_1(t-\tau)\frac{df_2(\tau)}{\mathrm{d}\tau}\mathrm{d}\tau. \tag{5}$$

The time-dependent stress or displacement boundary conditions under consideration are

$$\begin{aligned} \sigma_r \big|_{r=R_1(t)} &= p_1(t), \\ \sigma_r \big|_{r=R_2(t)} &= p_2(t), \end{aligned} \tag{6a}$$

or

$$\begin{aligned} u_r \big|_{r=R_1(t)} &= u_1(t), \\ u_r \big|_{r=R_2(t)} &= u_2(t), \end{aligned} \tag{6b}$$

where $p_1(t)$, $p_2(t)$ and $u_1(t)$, $u_2(t)$ are two pairs of prescribed functions of time.

3 Solution for the problem

3.1 The forms of solution in Laplace Space

Inserting Eq. (2) into (3), stress components can be expressed in terms of the radial displacement u_r as follows:

$$\begin{aligned} \sigma_r &= 2G(t) * d\left[\frac{2}{3}\frac{\partial u_r}{\partial r} - \frac{1}{3}\frac{u_r}{r}\right] + K(t) * d\left(\frac{\partial u_r}{\partial r} + \frac{u_r}{r}\right), \\ \sigma_\theta &= 2G(t) * d\left[\frac{2}{3}\frac{u_r}{r} - \frac{1}{3}\frac{\partial u_r}{\partial r}\right] + K(t) * d\left(\frac{\partial u_r}{\partial r} + \frac{u_r}{r}\right), \\ \sigma_z &= \left[K(t) - \frac{2}{3}G(t)\right] * d\left(\frac{\partial u_r}{\partial r} + \frac{u_r}{r}\right). \end{aligned} \tag{7}$$

Substituting the above equation into Eq. (1) yields the equation for displacement u_r as

$$\left[K(t) + \frac{4}{3}G(t)\right] * d\left(\frac{\partial^2 u_r}{\partial r^2} + \frac{1}{r}\frac{\partial u_r}{\partial r} - \frac{u_r}{r^2}\right) = 0. \tag{8}$$

According to the Laplace transform of a function $f(t)$, denoted by $\overline{f}(s)$, defined by

$$\overline{f}(s) = \int_0^\infty e^{-st} f(t)\mathrm{d}t,$$

where s is the transform parameter, and the inverse Laplace transform is expressed by

$$L^{-1}[\overline{f}(s)] = f(t) = \frac{1}{2\pi i}\int_{\beta - i\infty}^{\beta + i\infty} \overline{f}(s)e^{st}\mathrm{d}t,$$

the transform for Eq. (8) gives rise to

$$\left[\overline{K(t)} + \frac{4}{3}\overline{G(t)}\right] \cdot \left(\frac{\partial^2 u_r}{\partial r^2} + \frac{1}{r}\frac{\partial u_r}{\partial r} - \frac{u_r}{r^2}\right)_{t=0} + \left[\overline{K(t)} + \frac{4}{3}\overline{G(t)}\right] \cdot \overline{d\left(\frac{\partial^2 u_r}{\partial r^2} + \frac{1}{r}\frac{\partial u_r}{\partial r} - \frac{u_r}{r^2}\right)} = 0. \tag{9}$$

Note that

$$\overline{d\left(\frac{\partial^2 u_r}{\partial r^2} + \frac{1}{r}\frac{\partial u_r}{\partial r} - \frac{u_r}{r^2}\right)} = s\left(\frac{\partial^2 \overline{u_r}}{\partial r^2} + \frac{1}{r}\frac{\partial \overline{u_r}}{\partial r} - \frac{\overline{u_r}}{r^2}\right) - \left[\frac{\partial^2 u_r}{\partial r^2} + \frac{1}{r}\frac{\partial u_r}{\partial r} - \frac{u_r}{r^2}\right]_{t=0}. \tag{10}$$

Equation (9) simplifies to

$$\frac{\partial^2 \overline{u_r}}{\partial r^2} + \frac{1}{r}\frac{\partial \overline{u_r}}{\partial r} - \frac{\overline{u_r}}{r^2} = 0, \tag{11}$$

where $\overline{u_r}$ is a function of r and s. The general solution for Eq. (11) is

$$\overline{u_r} = \frac{A(s)}{r} + rB(s), \tag{12}$$

where $A(s)$ and $B(s)$ are two undetermined functions of the parameter s.

Next, the Laplace transform of Eq. (7) gives

$$\begin{aligned}
\overline{\sigma_r} &= \overline{2G(t)} \cdot s\left(\frac{2}{3}\frac{\partial \overline{u_r}}{\partial r} - \frac{1}{3}\frac{\overline{u_r}}{r}\right) + \overline{K(t)} \cdot s\left(\frac{\partial \overline{u_r}}{\partial r} + \frac{\overline{u_r}}{r}\right),\\
\overline{\sigma_\theta} &= \overline{2G(t)} \cdot s\left(\frac{2}{3}\frac{\overline{u_r}}{r} - \frac{1}{3}\frac{\partial \overline{u_r}}{\partial r}\right) + \overline{K(t)} \cdot s\left(\frac{\partial \overline{u_r}}{\partial r} + \frac{\overline{u_r}}{r}\right),\\
\overline{\sigma_z} &= \left[\overline{K(t)} - \frac{2}{3}\overline{G(t)}\right] s\left(\frac{\partial \overline{u_r}}{\partial r} + \frac{\overline{u_r}}{r}\right).
\end{aligned} \tag{13}$$

Using Eq. (12), Eq. (13) is rewritten as

$$\begin{aligned}
\overline{\sigma_r} &= \overline{2G(t)} \cdot s\left[-\frac{1}{r^2}A(s) + \frac{1}{3}B(s)\right] + 2\overline{K(t)} \cdot sB(s),\\
\overline{\sigma_\theta} &= \overline{2G(t)} \cdot s\left[\frac{1}{r^2}A(s) + \frac{1}{3}B(s)\right] + 2\overline{K(t)} \cdot sB(s),\\
\overline{\sigma_z} &= 2\left[\overline{K(t)} - \frac{2}{3}\overline{G(t)}\right] sB(s).
\end{aligned} \tag{14}$$

Equations (12) and (14) are the forms of solution for the stresses and displacement in Laplace space, which can be constructed by determining $A(s)$ and $B(s)$ based on the condition for time-dependent boundary regions in Eqs. (6a) or (6b).

3.2 Solution under stress boundary condition

Denote

$$C(t) = L^{-1}\left[\overline{G(t)} \cdot s \cdot A(s)\right], \tag{15}$$

$$D(t) = L^{-1}\left[\left(\frac{2}{3}\overline{G(t)} + 2\overline{K(t)}\right) B(s) \cdot s\right]. \tag{16}$$

In view of the first two equations in Eq. (14), the expressions for two in-plane stresses can be written by

$$\begin{aligned}
\sigma_r &= -\frac{2}{r^2}C(t) + D(t),\\
\sigma_\theta &= \frac{2}{r^2}C(t) + D(t).
\end{aligned} \tag{17}$$

According to the boundary condition (6a), there are

$$\begin{aligned}
-\frac{2}{R_1^2(t)}C(t) + D(t) &= p_1(t),\\
-\frac{2}{R_2^2(t)}C(t) + D(t) &= p_2(t),
\end{aligned}$$

which generates the solutions for $C(t)$ and $D(t)$:

$$C(t) = \frac{R_1^2(t)R_2^2(t)[p_2(t) - p_1(t)]}{2[R_2^2(t) - R_1^2(t)]},$$
$$D(t) = \frac{-p_1(t)R_1^2(t) + p_2(t)R_2^2(t)}{R_2^2(t) - R_1^2(t)}. \tag{18}$$

Substituting Eq. (18) into Eq. (17) gives the explicit form for two in-plane stresses in the following:

$$\sigma_r = -\frac{1}{r^2} \cdot \frac{R_1^2(t)R_2^2(t)[p_2(t) - p_1(t)]}{R_2^2(t) - R_1^2(t)} + \frac{-p_1(t)R_1^2(t) + p_2(t)R_2^2(t)}{R_2^2(t) - R_1^2(t)},$$
$$\sigma_\theta = \frac{1}{r^2} \cdot \frac{R_1^2(t)R_2^2(t)[p_2(t) - p_1(t)]}{R_2^2(t) - R_1^2(t)} + \frac{-p_1(t)R_1^2(t) + p_2(t)R_2^2(t)}{R_2^2(t) - R_1^2(t)}. \tag{19}$$

Further, the functions $A(s)$ and $B(s)$ are determined from Eqs. (15) and (16) as

$$A(s) = \frac{1}{\overline{G(t)} \cdot s} L\left\{\frac{R_1^2(t)R_2^2(t)[p_2(t) - p_1(t)]}{2[R_2^2(t) - R_1^2(t)]}\right\}, \tag{20}$$

$$B(s) = \frac{1}{s \cdot \left(\frac{2}{3}\overline{G(t)} + 2\overline{K(t)}\right)} L\left\{\frac{-p_1(t)R_1^2(t) + p_2(t)R_2^2(t)}{R_2^2(t) - R_1^2(t)}\right\}. \tag{21}$$

Using the inverse Laplace transform of Eq. (12) and the last equation in Eq. (14), the radial displacement and stress in the z-direction in the time domain can be expressed using $A(s)$ and $B(s)$ as

$$u_r = \frac{1}{r} L^{-1}[A(s)] + r L^{-1}[B(s)], \tag{22}$$

$$\sigma_z = 2L^{-1}[\overline{K(t)} s B(s)] - \frac{4}{3} L^{-1}[\overline{G(t)} s B(s)]. \tag{23}$$

By now, the solution for the axisymmetric problem with varying boundaries is derived in Eqs. (19), (20) and (21). In view of Eq. (19), it is clear that the two in-plane normal stress components are related to both time-dependent shape and external force, but they have no relation with the material parameters. The two stresses are, in form, similar to the case for time-independent boundary [6].

3.3 Solution under displacement boundary condition

In view of the resulting form of solution for the radial displacement in Eq. (22) or (12), two unknown time functions $L^{-1}[A(s)]$ and $L^{-1}[B(s)]$ can be determined using the boundary condition (6b) as

$$L^{-1}[A(s)] = f_1(t) = \frac{R_1(t) R_2(t) [u_1(t) R_2(t) - u_2(t) R_1(t)]}{R_2^2(t) - R_1^2(t)},$$
$$L^{-1}[B(s)] = f_2(t) = \frac{u_2(t) R_2(t) - u_1(t) R_1(t)}{R_2^2(t) - R_1^2(t)}, \tag{24}$$

then

$$u_r = \frac{1}{r} f_1(t) + r f_2(t). \tag{25}$$

The above equation shows that the radial displacement is related to both time-dependent shape and prescribed boundary displacements, but it also has no relation with the material parameters. Further, stress components are derived using Eqs. (14) and (24) in the following:

$$
\begin{aligned}
\sigma_r &= -\frac{2}{r^2}\int_0^t f_1(\tau)G'(t-\tau)\mathrm{d}\tau + \int_0^t f_2(\tau)\left[\frac{2}{3}G'(t-\tau)+2K'(t-\tau)\right]\mathrm{d}\tau \\
&\quad -\frac{2}{r^2}f_1(t)G(0) + f_2(t)\left[\frac{2}{3}G(0)+2K(0)\right], \\
\sigma_\theta &= \frac{2}{r^2}\int_0^t f_1(\tau)G'(t-\tau)\mathrm{d}\tau + \int_0^t f_2(\tau)\left[\frac{2}{3}G'(t-\tau)+2K'(t-\tau)\right]\mathrm{d}\tau \\
&\quad +\frac{2}{r^2}f_1(t)G(0) + f_2(t)\left[\frac{2}{3}G(0)+2K(0)\right], \\
\sigma_z &= \int_0^t f_2(\tau)\left[2K'(t-\tau)-\frac{4}{3}G'(t-\tau)\right]\mathrm{d}\tau + f_2(t)\left[2K(0)-\frac{4}{3}G(0)\right],
\end{aligned}
\tag{26}
$$

where $(\ )' = \frac{d(\ )}{d(t-\tau)}$.

4 Analysis of viscoelastic plane with varying circular hole under stress boundary condition

4.1 Case of infinite plane

In this section, explicit expressions for the above general solutions will be derived for an infinite viscoelastic plane problem involving a circular boundary having a time-dependent radius. This problem is of great importance in the area of rock mass construction. For the hole excavation in the infinite rock mass, due to the situation of section construction, the three-dimensional problem can reduce to a two-dimensional one concerning a plane perpendicular to the axis of the excavation. In some cases, e.g., deep tunnel excavation, there exist equivalent far-field compressive stresses in two directions, as shown in Fig. 2, where the inner radius $R_1 = R(t)$ is a function of time t, and stress σ_∞ at infinity may be constant or time-dependent. Boundary conditions for stress can be written by

$$
\begin{aligned}
\sigma_r \left|_{r=R(t)}\right. &= 0, \\
\sigma_r \left|_{r=\infty}\right. &= -\sigma_\infty(t).
\end{aligned}
\tag{27}
$$

According to Eq. (18), there are

$$
\begin{aligned}
C(t) &= -\frac{R^2(t)}{2}\sigma_\infty(t), \\
D(t) &= -\sigma_\infty(t).
\end{aligned}
\tag{28}
$$

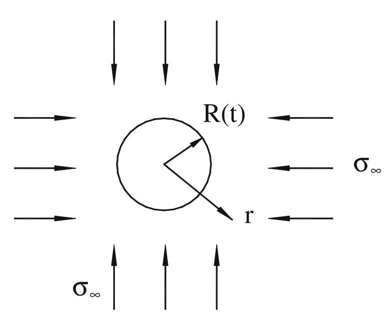

Fig. 2 Circular hole in infinite plane

Substituting the above equation into Eq. 19, the radial and circumferential stresses have the following results:

$$\begin{aligned}\sigma_r &= -\sigma_\infty(t)\left(1-\frac{R^2(t)}{r^2}\right),\\ \sigma_\theta &= -\sigma_\infty(t)\left(1+\frac{R^2(t)}{r^2}\right).\end{aligned} \tag{29}$$

4.1.1 Boltzmann viscoelastic model

It is assumed that the hydrostatic pressure (stress) at infinity is a constant of σ_0, i.e., $\sigma_\infty = \sigma_0$. The shear behavior of the material is governed using a Boltzmann viscoelastic model, as shown in Fig. 3, while the bulk behavior of the solid is prescribed to be purely elastic. The viscoelastic solid is thus characterized by two shear modulus G_{ve} and G_{e}, one viscosity coefficient η, and one bulk modulus K_{e}. The relaxation moduli in Eq. (3) are written

$$G(t) = \frac{G_{\mathrm{e}}^2}{G_{\mathrm{e}}+G_{\mathrm{ve}}}e^{-\frac{G_{\mathrm{e}}+G_{\mathrm{ve}}}{\eta}t} + \frac{G_{\mathrm{ve}}G_{\mathrm{e}}}{G_{\mathrm{e}}+G_{\mathrm{ve}}}, \quad K(t) = K_{\mathrm{e}}. \tag{30}$$

According to Eqs. (20) and (21), $A(s)$ and $B(s)$ can be determined as

$$A(s) = -\frac{\sigma_0}{2s}\frac{\overline{R^2(t)}}{\overline{G(t)}} = -\frac{\sigma_0}{2G_{\mathrm{e}}}L[R^2(t)]\left(1+\frac{G_{\mathrm{e}}}{\eta}\cdot\frac{1}{s+\frac{G_{\mathrm{ve}}}{\eta}}\right), \tag{31}$$

$$B(s) = -\frac{3\sigma_0}{2G_{\mathrm{e}}+6K_{\mathrm{e}}}\cdot\frac{1}{s+\left[\frac{G_{\mathrm{ve}}}{\eta}+\frac{3K_{\mathrm{e}}G_{\mathrm{e}}}{\eta(G_{\mathrm{e}}+3K_{\mathrm{e}})}\right]} - \frac{3(G_{\mathrm{e}}+G_{\mathrm{ve}})\sigma_0}{\eta(2G_{\mathrm{e}}+6K_{\mathrm{e}})}\cdot\frac{1}{s}\cdot\frac{1}{s+\left[\frac{G_{\mathrm{ve}}}{\eta}+\frac{3K_{\mathrm{e}}G_{\mathrm{e}}}{\eta(G_{\mathrm{e}}+3K_{\mathrm{e}})}\right]}, \tag{32}$$

and their inversions into the time domain are derived as

$$L^{-1}[A(s)] = -\frac{\sigma_0}{2G_{\mathrm{e}}}R^2(t) - \frac{\sigma_0}{2\eta}e^{-\frac{G_{\mathrm{ve}}}{\eta}t}\int_0^t R^2(t)e^{\frac{G_{\mathrm{ve}}}{\eta}t}\mathrm{d}t, \tag{33}$$

$$\begin{aligned}L^{-1}[B(s)] = &-\frac{3\sigma_0}{2G_{\mathrm{e}}+6K_{\mathrm{e}}}\cdot e^{-\frac{G_{\mathrm{ve}}}{\eta}t}\cdot e^{-\frac{3K_{\mathrm{e}}G_{\mathrm{e}}}{(G_{\mathrm{e}}+3K_{\mathrm{e}})\eta}t} - \frac{3(G_{\mathrm{e}}+G_{\mathrm{ve}})\sigma_0}{2(G_{\mathrm{e}}G_{\mathrm{ve}}+3K_{\mathrm{e}}G_{\mathrm{e}}+3K_{\mathrm{e}}G_{\mathrm{ve}})}\\ &\times\left(1-e^{-\frac{G_{\mathrm{ve}}}{\eta}t}\cdot e^{-\frac{3K_{\mathrm{e}}G_{\mathrm{e}}}{(G_{\mathrm{e}}+3K_{\mathrm{e}})\eta}t}\right).\end{aligned} \tag{34}$$

Further, substitution of Eqs. (33) and (34) into Eqs. (22) and (23) yields

$$\begin{aligned}u_r = &-\frac{\sigma_0}{2G_{\mathrm{e}}r}R^2(t) - \frac{\sigma_0}{2\eta r}e^{-\frac{G_{\mathrm{ve}}}{\eta}t}\int_0^t R^2(t)e^{\frac{G_{\mathrm{ve}}}{\eta}t}\mathrm{d}t - \frac{3\sigma_0 r}{2G_{\mathrm{e}}+6K_{\mathrm{e}}}\cdot e^{-\frac{G_{\mathrm{ve}}}{\eta}t}\cdot e^{-\frac{3K_{\mathrm{e}}G_{\mathrm{e}}}{(G_{\mathrm{e}}+3K_{\mathrm{e}})\eta}t}\\ &-\frac{3(G_{\mathrm{e}}+G_{\mathrm{ve}})\sigma_0 r}{2(G_{\mathrm{e}}G_{\mathrm{ve}}+3K_{\mathrm{e}}G_{\mathrm{e}}+3K_{\mathrm{e}}G_{\mathrm{ve}})}\left(1-e^{-\frac{G_{\mathrm{ve}}}{\eta}t}\cdot e^{-\frac{3K_{\mathrm{e}}G_{\mathrm{e}}}{(G_{\mathrm{e}}+3K_{\mathrm{e}})\eta}t}\right),\end{aligned} \tag{35}$$

$$\sigma_z = -\sigma_0 + \frac{3G_{\mathrm{e}}\sigma_0}{G_{\mathrm{e}}+3K_{\mathrm{e}}}e^{-\frac{G_{\mathrm{ve}}}{\eta}t}\cdot e^{-\frac{3K_{\mathrm{e}}G_{\mathrm{e}}}{(G_{\mathrm{e}}+3K_{\mathrm{e}})\eta}t} + \frac{3G_{\mathrm{e}}G_{\mathrm{ve}}\sigma_0}{G_{\mathrm{e}}G_{\mathrm{ve}}+3K_{\mathrm{e}}G_{\mathrm{ve}}+3K_{\mathrm{e}}G_{\mathrm{e}}}\left(1-e^{-\frac{G_{\mathrm{ve}}}{\eta}t}\cdot e^{-\frac{3K_{\mathrm{e}}G_{\mathrm{e}}}{(G_{\mathrm{e}}+3K_{\mathrm{e}})\eta}t}\right). \tag{36}$$

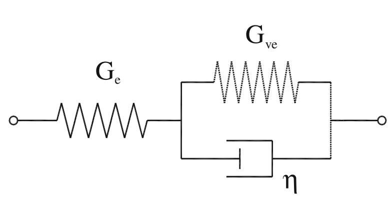

Fig. 3 Boltzmann viscoelastic model

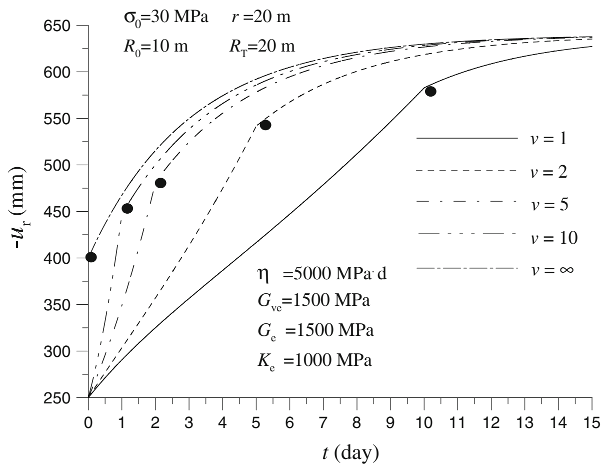

Fig. 4 Displacement response for different values of the velocity for the case of infinite plane

The varying radius is assumed to have the following form:

$$R(t)=\begin{cases} R_0+vt & 0\le t\le T,\\ R_T & t>T,\end{cases} \tag{37}$$

where T and v are ending time and velocity of change in the radius, respectively. R_0 and R_T represent initial and ending radii, respectively. The radial displacement in Eq. (35) can be expressed finally in an explicit form as

$$\begin{aligned} u_r(r,t)=&-\frac{\sigma_0}{2G_\mathrm{e}r}(R_0+vt)^2-\frac{\sigma_0R_0^2}{2G_\mathrm{ve}r}\left(1-e^{-\frac{G_\mathrm{ve}}{\eta}t}\right)-\frac{\sigma_0R_0v}{G_\mathrm{ve}r}t+\frac{\sigma_0R_0v}{G_\mathrm{ve}^2r}\eta\cdot\left(1-e^{-\frac{G_\mathrm{ve}}{\eta}t}\right)\\ &-\frac{\sigma_0v^2}{2G_\mathrm{ve}r}t^2+\frac{\sigma_0v^2\eta}{G_\mathrm{ve}^2r}t-\frac{\sigma_0v^2\eta^2}{G_\mathrm{ve}^3r}\cdot\left(1-e^{-\frac{G_\mathrm{ve}}{\eta}t}\right)-\frac{3\sigma_0r}{2G_\mathrm{e}+6K_\mathrm{e}}\cdot e^{-\frac{G_\mathrm{ve}}{\eta}t}\cdot e^{-\frac{3K_\mathrm{e}G_\mathrm{e}}{(G_\mathrm{e}+3K_\mathrm{e})\eta}t}\\ &-\frac{3(G_\mathrm{e}+G_\mathrm{ve})\sigma_0r}{2(G_\mathrm{e}G_\mathrm{ve}+3K_\mathrm{e}G_\mathrm{e}+3K_\mathrm{e}G_\mathrm{ve})}\left(1-e^{-\frac{G_\mathrm{ve}}{\eta}t}\cdot e^{-\frac{3K_\mathrm{e}G_\mathrm{e}}{(G_\mathrm{e}+3K_\mathrm{e})\eta}t}\right) \end{aligned} \tag{38}$$

for $0\le t\le T$, and

$$\begin{aligned} u_r(r,t)=&-\frac{\sigma_0}{2G_\mathrm{e}r}R_T^2-\frac{\sigma_0}{2G_\mathrm{ve}r}R_0^2\left[e^{\frac{G_\mathrm{ve}}{\eta}(T-t)}-e^{-\frac{G_\mathrm{ve}}{\eta}t}\right]-\frac{\sigma_0R_0v}{G_\mathrm{ve}r}T\cdot e^{\frac{G_\mathrm{ve}}{\eta}(T-t)}\\ &+\frac{\sigma_0R_0v\eta}{G_\mathrm{ve}^2r}\cdot\left[e^{\frac{G_\mathrm{ve}}{\eta}(T-t)}-e^{-\frac{G_\mathrm{ve}}{\eta}t}\right]-\frac{\sigma_0v^2}{2G_\mathrm{ve}r}T^2e^{\frac{G_\mathrm{ve}}{\eta}(T-t)}+\frac{\sigma_0v^2\eta}{G_\mathrm{ve}^2r}T\cdot e^{\frac{G_\mathrm{ve}}{\eta}(T-t)}\\ &-\frac{\sigma_0v^2\eta^2}{G_\mathrm{ve}^3r}\cdot\left[e^{\frac{G_\mathrm{ve}}{\eta}(T-t)}-e^{-\frac{G_\mathrm{ve}}{\eta}t}\right]-\frac{\sigma_0R_T^2}{2G_\mathrm{ve}r}\left[1-e^{\frac{G_\mathrm{ve}}{\eta}(T-t)}\right]-\frac{3\sigma_0r}{2G_\mathrm{e}+6K_\mathrm{e}}\cdot e^{-\frac{G_\mathrm{ve}}{\eta}t}\cdot e^{-\frac{3K_\mathrm{e}G_\mathrm{e}}{(G_\mathrm{e}+3K_\mathrm{e})\eta}t}\\ &-\frac{3(G_\mathrm{e}+G_\mathrm{ve})\sigma_0r}{2(G_\mathrm{e}G_\mathrm{ve}+3K_\mathrm{e}G_\mathrm{e}+3K_\mathrm{e}G_\mathrm{ve})}\left(1-e^{-\frac{G_\mathrm{ve}}{\eta}t}\cdot e^{-\frac{3K_\mathrm{e}G_\mathrm{e}}{(G_\mathrm{e}+3K_\mathrm{e})\eta}t}\right) \end{aligned} \tag{39}$$

for $t>T$.

In computation, the properties of the viscoelastic material are chosen as $G_\mathrm{e}=1{,}500$ MPa, $G_\mathrm{ve}=1{,}500$ MPa, $K_\mathrm{e}=1{,}000$ MPa and $\eta=5{,}000$ MPa $\cdot$ d, where d represents time "day" as a unit of time used in the excavation process. The stress at infinity and two radii are prescribed as $\sigma_0=30$ MPa and $R_0=10$ m, $R_T=20$ m, respectively. The displacement response at $r=30$ m for different values of the velocity is illustrated in Fig. 4. The dot points in the figure represent the positions at the ending time of varying radius. The results show that there is rapid increase in the displacement prior to the ending times T for different values of v, and a smaller value for the velocity causes a larger value of displacement when $t=T$. Furthermore, a smaller value of velocity of change in the radius corresponds to a shorter time during which the response tends to be stable.

4.1.2 Maxwell viscoelastic model

Suppose that a viscoealstic plane region containing a circular hole is subject to a time-dependent stress at infinity having a sinusoidal form as follows:

$$\sigma_\infty(t) = \sigma_0 + \sigma_1 \sin\omega t, \tag{40}$$

where σ_0 and σ_1 are two constants, and ω is the circular frequency. For the Maxwell viscoelastic material, as shown in Fig. 5, two relaxation moduli are written as

$$G(t) = G_e e^{-\frac{G_e}{\eta}t}, \quad K(t) = K_e, \tag{41}$$

where G_e and K_e are the shear modulus and bulk modulus, respectively. $A(s)$ and $B(s)$ in Eqs. (20) and (21) can be thus determined as

$$A(s) = -\frac{\sigma_0}{2G_e} L[R^2(t)]\left(1 + \frac{G_e}{\eta\, s}\right) - \frac{\sigma_1}{2G_e} L[R^2(t)\sin\omega t]\left(1 + \frac{G_e}{\eta\, s}\right), \tag{42}$$

$$B(s) = \frac{-3\sigma_0}{2(G_e + 3K_e)} \cdot \frac{1}{s + d_1} - \frac{3\sigma_0 G_e}{2\eta(G_e + 3K_e)} \frac{1}{s(s + d_1)} - \frac{3\sigma_1\omega}{2(G_e + 3K_e)}\left(\frac{C_1 s + C_2}{s^2 + \omega^2} - \frac{C_1}{s + d_1}\right), \tag{43}$$

where

$$\begin{aligned} d_1 &= \frac{3K_e G_e}{\eta(G_e + 3K_e)}, \quad d_2 = \frac{G_e}{\eta}, \\ C_1 &= \frac{d_1 - d_2}{d_1^2 + \omega^2}, \quad C_2 = \frac{\omega^2 + d_1 d_2}{d_1^2 + \omega^2}. \end{aligned} \tag{44}$$

Making the inverse Laplace transform for Eqs. (42) and (43), substituting the resulting $L^{-1}[A(s)]$ and $L^{-1}[B(s)]$ into Eq. (22) finally yields

$$\begin{aligned} u_r = &-\frac{\sigma_0}{2G_e r} R^2(t) - \frac{\sigma_0}{2\eta r}\int_0^t R^2(t)\mathrm{d}t - \frac{\sigma_1}{2G_e r} R^2(t)\cdot\sin\omega t - \frac{\sigma_1}{2\eta r}\int_0^t R^2(t)\cdot\sin\omega t\mathrm{d}t \\ &-\frac{\sigma_0\cdot r}{2K_e} + \frac{\sigma_0 G_e\cdot r}{2K_e(G_e + 3K_e)}\cdot e^{-d_1 t} - \frac{3\sigma_1\omega\cdot r}{2(G_e + 3K_e)}\left(C_1\cos\omega t + \frac{C_2}{\omega}\sin\omega t - C_1 e^{-d_1 t}\right). \end{aligned} \tag{45}$$

For the special case of impressive materials under uniform pressure at infinity, $K_e \to \infty$, $\sigma_1 = 0$, the above equations for the displacement and stresses determined by Eqs. (45) and (29) reduce to the known results [31].

If the varying radius takes the form of $R(t) = R_0 + vt$, the radial displacement can be evaluated using the following formula:

$$\begin{aligned} u_r = &-\frac{\sigma_0}{2G_e r}(R_0 + vt)^2 - \frac{\sigma_0}{2\eta r}\left(R_0^2 + R_0 vt + \frac{1}{3}v^2 t^2\right) - \frac{\sigma_1}{2G_e r}(R_0 + vt)^2\cdot\sin\omega t - \frac{\sigma_1}{2\eta r}C_3 \\ &-\frac{\sigma_0\cdot r}{2K_e} + \frac{\sigma_0 G_e\cdot r}{2K_e(G_e + 3K_e)}\cdot e^{-d_1 t} - \frac{3\sigma_1\omega\cdot r}{2(G_e + 3K_e)}\left(C_1\cos\omega t + \frac{C_2}{\omega}\sin\omega t - C_1 e^{-d_1 t}\right), \end{aligned} \tag{46}$$

where

$$C_3 = \frac{R_0^2}{\omega}(1 - \cos\omega t) + \frac{2R_0 v}{\omega}\left(\frac{1}{\omega}\sin\omega t - t\cos\omega t\right) + \frac{v^2}{\omega}\left(\frac{2}{\omega}t\sin\omega t + \frac{2}{\omega^2}\cos\omega t - t^2\cos\omega t - \frac{2}{\omega^2}\right). \tag{47}$$

Fig. 5 Maxwell viscoelastic model

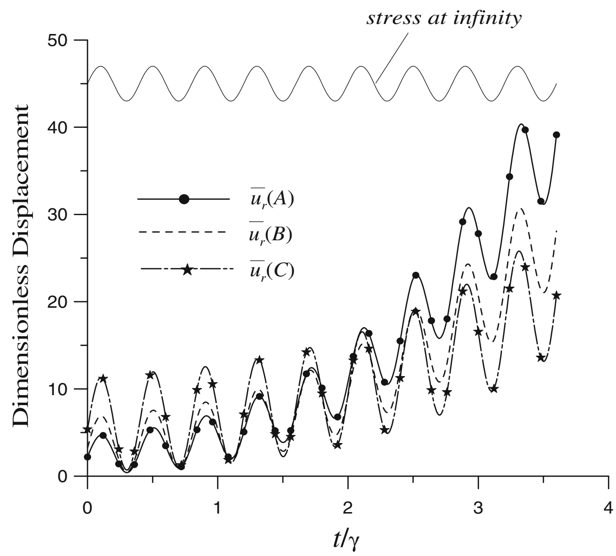

Fig. 6 Displacement responses at different locations

Next, let $\sigma_1 = \sigma_0$ in Eq. (40), and the following values of properties of viscoelastic material and the circular frequency are used for an example:

$$\frac{G_e}{\sigma_0} = 1 \times 10^3, \quad \frac{K_e}{\sigma_0} = 2 \times 10^3, \quad \frac{\eta}{\sigma_0} = 5 \times 10^2 \ (d), \quad \omega = 2\pi \left(d^{-1}\right).$$

The responses for the radial displacement are displayed in Fig. 6 at locations for three different values of the radial coordinate r, i.e., Points A $(r/R_0 = 10)$, B $(r/R_0 = 15)$ and C $(r/R_0 = 25)$ inside the viscoelastic domain. In computation the time and displacement have been normalized by the relaxation time, $\gamma = \eta/G_e$, and the initial radius, $R_0 \left(\times 10^{-3}\right)$, respectively. It is observed that the displacement increases with time in a form of fluctuation and tends to infinity, which reflects the property of liquid-like deformation of the material due to the Maxwell model. The results also show that the increase in the displacement for a farther point is comparatively slower.

4.2 Case of finite plane

To illustrate the effect of finite outer radius R_2 on viscoelastic fields induced by boundary constant stresses p_1 and p_2, we introduce an aspect ratio characterizing the volume concentration of the cylindrical void:

$$c_v = \frac{R_1^2}{R_2^2}, \tag{48}$$

then Eq. (18) changes to $C(t) = \frac{R_1^2(p_2 - p_1)}{2(1-c_v)}$, $D(t) = \frac{-p_1 c_v + p_2}{1-c_v}$. For the case of the Boltzmann model, Eqs. (20) and (21) change to

$$A(s) = \frac{1}{2G_e}\left(1 + \frac{G_e}{\eta} \cdot \frac{1}{s + \frac{G_{ve}}{\eta}}\right) L\left[\frac{R_1^2(p_2 - p_1)}{2(1 - c_v)}\right], \tag{49}$$

$$B(s) = \left[\frac{3}{2G_e + 6K_e} + \frac{3G_e^2}{2(G_e + 3K_e)^2\eta} \cdot \frac{1}{s + \frac{1}{\eta}\left(G_{ve} + \frac{3K_e G_e}{G_e + 3K_e}\right)}\right] L\left[\frac{-p_1 c_v + p_2}{1 - c_v}\right], \tag{50}$$

Table 1 Inner and outer radii in computation

No.	R_2 (m)	$R_1(t)=\begin{cases} R_0+vt & 0\le t\le T \\ R_T & t>T \end{cases}$			
		R_0	v (m/day)	R_T (m)	T (day)
1	40.0	10.0	1.0	20.0	10
2	60.0				
3	90.0				
4	120.0				

the inversions are

$$L^{-1}[A(s)]=\frac{1}{2G_{\mathrm{e}}}\cdot\frac{R_1^2(p_2-p_1)}{2(1-c_v)}+\frac{1}{2\eta}\cdot e^{-\frac{G_{\mathrm{ve}}}{\eta}t}\int_0^t\frac{R_1^2(p_2-p_1)}{2(1-c_v)}\cdot e^{\frac{G_{\mathrm{ve}}}{\eta}t}\mathrm{d}t, \tag{51}$$

$$L^{-1}[B(s)]=\frac{3}{2G_{\mathrm{e}}+6K_{\mathrm{e}}}\cdot\frac{-p_1\cdot c_v+p_2}{1-c_v}+\frac{3G_{\mathrm{e}}^2}{2(G_{\mathrm{e}}+3K_{\mathrm{e}})^2\eta}\cdot e^{-at}\cdot\int_0^t\frac{-p_1\cdot c_v+p_2}{1-c_v}\cdot e^{at}\mathrm{d}t, \tag{52}$$

where $a=\frac{1}{\eta}(G_{\mathrm{ve}}+\frac{3K_{\mathrm{e}}G_{\mathrm{e}}}{G_{\mathrm{e}}+3K_{\mathrm{e}}})$. Using Eq. (22) together with Eqs. (51) and (52), the radial displacement can be written as

$$u_r=\frac{1}{r}\left[\frac{1}{4G_{\mathrm{e}}}\cdot\frac{R_1^2(p_2-p_1)}{1-c_v}+\frac{1}{4\eta}\cdot e^{-\frac{G_{\mathrm{ve}}}{\eta}t}\int_0^t\frac{R_1^2(p_2-p_1)}{1-c_v}\cdot e^{\frac{G_{\mathrm{ve}}}{\eta}t}\mathrm{d}t\right]$$
$$+r\left[\frac{3}{2G_{\mathrm{e}}+6K_{\mathrm{e}}}\cdot\frac{-p_1\cdot c_v+p_2}{1-c_v}+\frac{3G_{\mathrm{e}}^2}{2(G_{\mathrm{e}}+3K_{\mathrm{e}})^2\eta}\cdot e^{-at}\cdot\int_0^t\frac{-p_1\cdot c_v+p_2}{1-c_v}\cdot e^{at}\mathrm{d}t\right]. \tag{53}$$

The above equation can be used to evaluate the effect of the aspect ratio c_v. Especially, if $p_1=0$, $p_2=-\sigma_0$ (pressure) for the case of infinite plane ($c_v\to 0$), the above equation will reduce to Eq. (35).

For the sake of calculation, the inner radius is assumed to be the form in Eq. (37), the parameters in computation are listed in Table 1 while material parameters are given in Sect. 4.1.1. The values of two boundary stresses are chosen as $p_2=30$ MPa and $p_1=0$. For various values of R_2, the variation of the aspect ratio c_v as a function of time t is presented in Fig. 7. The changes in the radial displacement at the location $r=20$ m with time and the ratio are displayed in Figs. 8 and 9, respectively. The calculations show that similar to the case of an infinite plane, there is a rapid increase in the displacement prior to the ending times T, as shown in Fig. 8. A smaller outer radius R_2 (also a larger ratio c_v) causes a larger value of displacement. The results reveal that the response tends to be stable at the same times for different ratio as the velocity of change keeps unchanged ($v=1$). It is observed from Fig. 9 that the displacement increases with an increasing ratio, and there is a wider scope of change in the ratio inducing the increasing response for a smaller R_2. In addition, the segment of straight lines in the figure presents an increase in the displacement with time although the aspect ratio keeps unchanged.

5 Analysis of viscoelastic plane with varying circular hole under displacement boundary condition

5.1 Case of infinite plane

Consider the displacement boundary condition for the case of $R_2\to\infty$ and $R_1=R(t)$ below:

$$\begin{aligned} u_r\big|_{r=R(t)} &= u_1, \\ u_r\big|_{r=\infty} &= 0, \end{aligned} \tag{54}$$

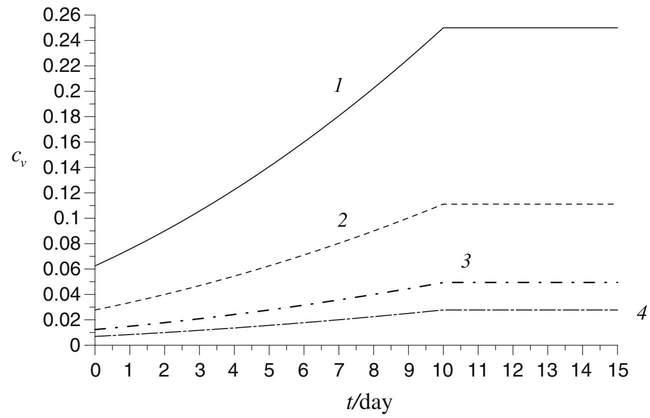

Fig. 7 Change in aspect ratio with time

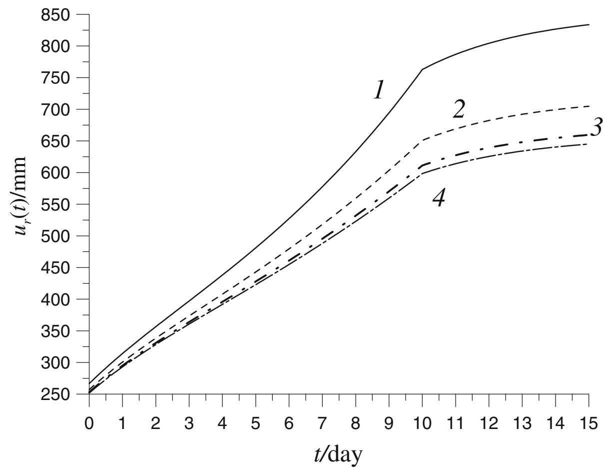

Fig. 8 Change in the radial displacement with time for different outer radius

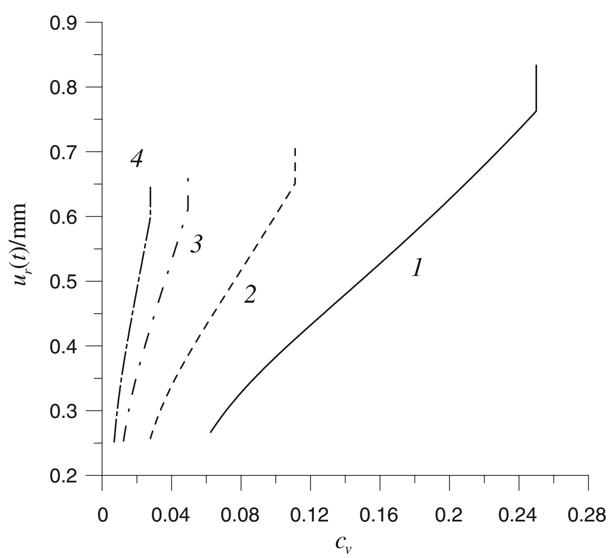

Fig. 9 Change in the radial displacement with the ratio

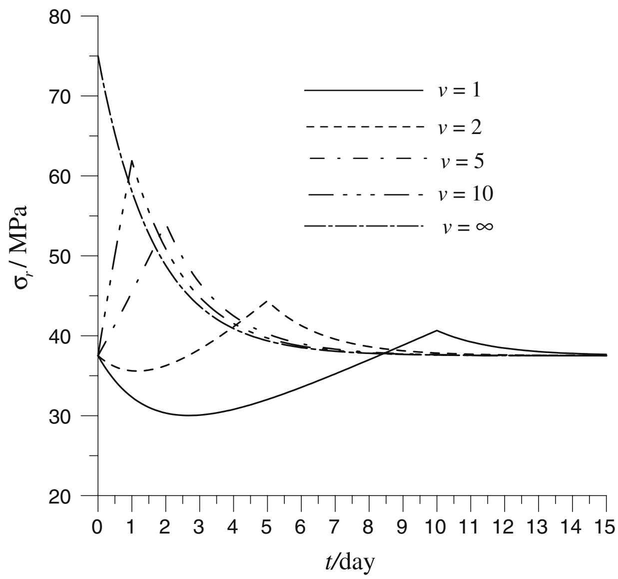

Fig. 10 Change in the radial stress with time for different velocities

where u_1 is assumed to be unchanged with time. Using Eq. (54), Eq. (24) reduces to

$$f_1(t) = R(t) \cdot u_1, \quad f_2(t) = 0. \tag{55}$$

Employing the Boltzmann model in Eq. (30), the stress components are derived using Eq. (26) as

$$\begin{cases} \sigma_r \\ \sigma_\theta \end{cases} = \pm \frac{2}{r^2} \int_0^t (R_0 + v\tau) u_1 \cdot \frac{G_e^2}{\eta} e^{-\frac{G_e + G_{ve}}{\eta}(t-\tau)} \mathrm{d}\tau \mp \frac{2}{r^2} (R_0 + v\tau) u_1 G_e,$$
$$\sigma_z = 0 \tag{56}$$

for $0 \le t \le T$, and

$$\begin{cases} \sigma_r \\ \sigma_\theta \end{cases} = \pm \frac{2}{r^2} \int_0^T (R_0 + v\tau) u_1 \cdot \frac{G_e^2}{\eta} e^{-\frac{G_e + G_{ve}}{\eta}(t-\tau)} \mathrm{d}\tau \pm \frac{2}{r^2} \int_T^t R_T u_1 \cdot \frac{G_e^2}{\eta} e^{-\frac{G_e + G_{ve}}{\eta}(t-\tau)} \mathrm{d}\tau \mp \frac{2}{r^2} R_T u_1 G_e,$$
$$\sigma_z = 0 \tag{57}$$

for $t > T$.

In the above derivation, Eq. (37) for the inner radius is applied. In computation, it is assumed that $u_1 = -0.5$ m, $R_0 = 10$ m, $R_T = 20$ m, using material parameters as described in Sect. 4.1.1, and the change in the radial stress at a location $r = 20$ m with time is displayed for various velocities for excavation in Fig. 10. As shown in the figure, for smaller values of the velocity, the stress first has a drop in the excavation process, and then increases to a peak value at a time corresponding to the observation location. However, when the velocity for excavation is large, the stress increases to its peak value without a clear initial drop. A lower velocity results in a smaller peak value of the stress, which arrives at a later time.

5.2 Case of finite plane

Consider the boundary condition with finite outer radius R_2:

$$u_r \big|_{r=R(t)} = u_1,$$
$$u_r \big|_{r=R_2} = 0, \tag{58}$$

where u_1 is prescribed as a constant value. Eq. (24) thus simplifies into

$$f_1(t) = \frac{R(t)\cdot u_1}{1-c_v}, \quad f_2(t) = \frac{-c_v\cdot u_1}{(1-c_v)R_1}. \tag{59}$$

Due to the Boltzmann model, the corresponding stress components are expressed using Eqs. (26) and Eq. (58) in the following:

$$\begin{cases} \sigma_r \\ \sigma_\theta \end{cases} = \pm\frac{2}{r^2}\int_0^t \frac{(R_0+v\tau)R_2^2u_1}{R_2^2-(R_0+v\tau)^2}\cdot\frac{G_e^2}{\eta}e^{-\frac{G_e+G_{ve}}{\eta}(t-\tau)}d\tau + \int_0^t \frac{(R_0+v\tau)u_1}{R_2^2-(R_0+v\tau)^2}\cdot\frac{2G_e^2}{3\eta}e^{-\frac{G_e+G_{ve}}{\eta}(t-\tau)}d\tau$$
$$\mp\frac{2}{r^2}\frac{(R_0+vt)R_2^2u_1}{R_2^2-(R_0+vt)^2}\cdot G_e - \frac{(R_0+vt)u_1}{R_2^2-(R_0+vt)^2}\frac{2}{3}G_e, \tag{60}$$
$$\sigma_z = 0$$

for $0 \le t \le T$, and

$$\begin{cases} \sigma_r \\ \sigma_\theta \end{cases} = \pm\frac{2}{r^2}\int_0^T \frac{(R_0+v\tau)R_2^2u_1}{R_2^2-(R_0+v\tau)^2}\cdot\frac{G_e^2}{\eta}e^{-\frac{G_e+G_{ve}}{\eta}(t-\tau)}d\tau \pm \frac{2}{r^2}\int_T^t \frac{R_TR_2^2u_1}{R_2^2-R_T^2}\cdot\frac{G_e^2}{\eta}e^{-\frac{G_e+G_{ve}}{\eta}(t-\tau)}d\tau$$
$$+\int_0^T \frac{(R_0+v\tau)u_1}{R_2^2-(R_0+v\tau)^2}\cdot\frac{2G_e^2}{3\eta}e^{-\frac{G_e+G_{ve}}{\eta}(t-\tau)}d\tau + \int_T^t \frac{R_T\cdot u_1}{R_2^2-R_T^2}\cdot\frac{2G_e^2}{3\eta}e^{-\frac{G_e+G_{ve}}{\eta}(t-\tau)}d\tau \tag{61}$$
$$\mp\frac{2}{r^2}\frac{R_TR_2^2u_1}{R_2^2-R_T^2}\cdot G_e - \frac{R_Tu_1}{R_2^2-R_T^2}\frac{2}{3}G_e,$$
$$\sigma_z = 0$$

for $t > T$. Especially, when $R_2 \to \infty$ or $c_v \to 0$, the above Eqs. (60) and (61) will degenerate into Eqs. (56) and (57), respectively, for the case of an infinite plane.

As a numerical example, a time history of the radial stress at the location $r = 20$ m for $v = 1$ is shown for various values of R_2 in Fig. 11 while the stress changes with the ratio c_v in Fig. 12. It is seen from Fig. 11 that, during the early period of the excavation, there is a drop in the stress, which is similar to the case of an infinite plane. A smaller R_2 (also a larger c_v) induces a higher stress at the same time. Meanwhile, the segment of straight lines, as shown in Fig. 12, presents a decrease in stress with time when the aspect ratio keeps unchanged.

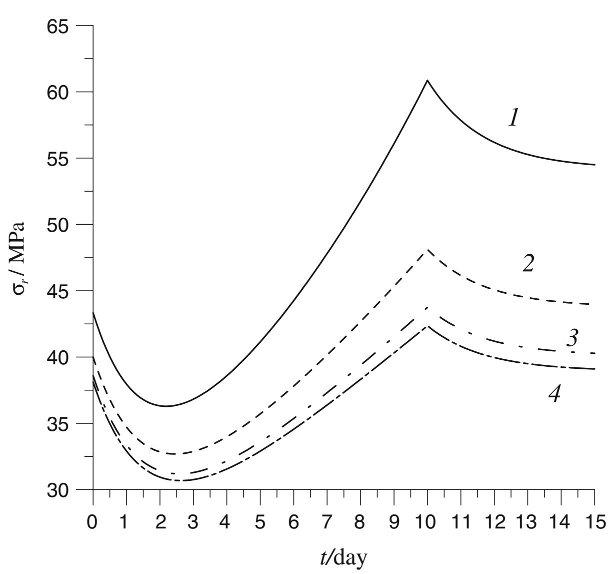

Fig. 11 Change in the radial stress with time for different outer radius

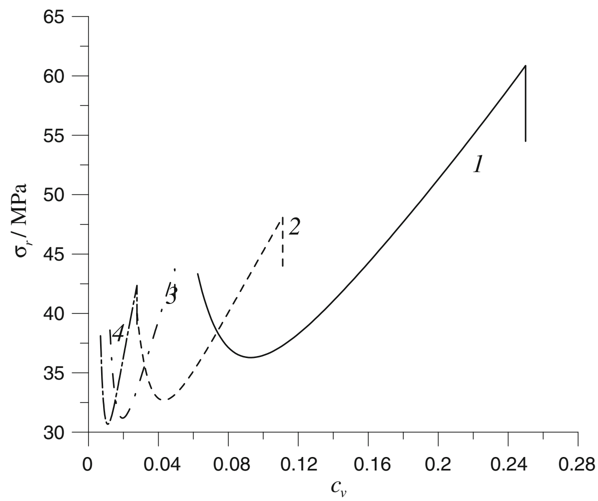

Fig. 12 Change in the stress with the ratio for different outer radius

6 Conclusions

The analytical solutions for viscoelastic axisymmetric plane problems involving time-dependent boundary regions are presented using the Laplace transform. The explicit expressions are given for the radial and circumferential stresses under stress boundary condition and the radial displacement under displacement boundary condition. The results indicate that the two in-plane stress components and the displacement under corresponding boundary conditions have no relation with material constants, which is similar to the case for time-independent boundary. The general form of solutions for remaining displacement or stress field is expressed by the inverse Laplace transform concerning two relaxation moduli. Numerical examples for a circular hole subject to axisymmetric time-dependent stress or displacement are given to illustrate the displacement and stress response in excavation or void growth.

The results show that, using the Boltzmann viscoelastic model, if the radius varies slowly, the displacement response under stress boundary condition greatly increases with time, but is larger at the end of varying time. So it is necessary to support the tunnel during the excavation and to excavate as soon as possible. For the Maxwell model, the displacement increases with time in a form of fluctuation and tends to infinity, which reflects the liquid-like deformation of the material. In addition, for the case of a finite plane, a smaller outer radius (also a larger aspect ratio) causes a larger displacement response using the Boltzmann model, and corresponds to a wider scope of change in the ratio generating the increasing displacement response. In contrast, for the case of displacement boundary condition, there is a drop in the radial stress during an early period of excavation (or void growth) based on the Boltzmann model, which then increases to a peak value. A lower velocity results in a smaller peak value of the stress, which arrives at a later time. A smaller outer radius produces a higher stress at the same time, and also corresponds to a wider scope of change in the ratio causing the increasing stress response.

The method proposed in this paper can be suitable for the analysis of earth excavation and finite void growth.

Acknowledgements This work is supported by National Natural Science Foundation of China through Grant No.10702052. The authors thank the reviewers for valuable comments and suggestions for improving the presentation of the paper.

References

1. Gurtin, M.E., Sternberg, E.: On the linear theory of viscoelasticity. Arch. Ration. Mech. Anal. **11**, 291–356 (1962)
2. Bernstein, B., Kearsley, E.A., Zapas, L.J.: A study of stress relaxation with finite strains. Trans. Soc. Rheol. **7**, 391–409 (1963)
3. McGuirt, C.W., Lianis, G.: Constitutive equations for viscoelastic solids under finite uniaxial and biaxial deformations. Trans. Soc. Rheol. **14**, 117–134 (1970)
4. Pipkin, A.C., Rogers, T.G.: A nonlinear integral representation for viscoelastic behavior. J. Mech. Phys. Solids **16**, 59–72 (1968)

5. Schapery, R.A.: On the characterization of non-linear viscoelastic materials. Polym. Eng. Sci. **9**, 295–310 (1969)
6. Flügge, W.: Viscoelasticity, 2nd edn. Springer, New York (1975)
7. Findley, W.N., Lai, J.S., Onaran, K.: Creep and relaxation of non-linear viscoelastic materials. North-Holland, Amsterdam (1976)
8. Weng, G.J.: A physically consistent method for the prediction of creep behavior of metals. J. Appl. Mech. **46**, 800–804 (1979)
9. Weng, G.J.: Self-consistent determination of time-dependent behavior of metals. J. Appl. Mech. **48**, 41–46 (1981)
10. Weng, G.J.: A self-consistent scheme for the relaxation behavior of metals. J. Appl. Mech. **48**, 779–784 (1981)
11. Weng, G.J.: A unified, self-consistent theory for the plastic-creep deformation of metals. J. Appl. Mech. **49**, 728–734 (1982)
12. Weng, G.J.: Cyclic stress relaxation of polycrystalline metals at elevated temperature. Int. J. Solids Struct. **19**, 541–551 (1983)
13. Weng, G.J.: Tensile creep acceleration by superimposed cyclic torsional strain in polycrystalline metals. Mater. Sci. Eng. **57**, 127–133 (1983)
14. Christensen, R.M.: A nonlinear theory of viscoelasticity for application to Elastomers. J. Appl. Mech. **47**, 762–768 (1980)
15. Christensen, R.M.: Theory of Viscoelasticity: an introduction, 2nd edn. Academic Press, New York (1982)
16. Graham, G.A.C.: The correspondence principle of linear viscoelasticity theory for mixed boundary value problems involving time-dependent boundary regions. Q. Appl. Math. **26**, 167–174 (1968)
17. Graham, G.A.C., Sabin, G.C.W.: The correspondence principle of linear viscoelasticity for problems that involve time-dependent regions. Int. J. Eng. Sci. **11**, 123–140 (1973)
18. Graham, G.A.C.: The solution of mixed boundary value problems that involve time-dependent boundary regions for viscoelastic materials with one relaxation function. Acta Mech. **8**, 188–204 (1969)
19. Lee, E.H.: Stress analysis in viscoelastic bodies. Q. Appl. Math. **13**, 183 (1955)
20. Barrett, K.E., Gotts, A.C.: 2-D finite element analysis of a compressible dynamic viscoelastic cylinder using FFT. Commun. Numer. Meth. Eng. **18**, 729–742 (2002)
21. Mana, A.I., Clough, G.W.: Prediction of movements for braced cuts in clay. J. Geotech. Eng. Div. ASCE **107**, 759–778 (1981)
22. Rashba, E.I.: Stress determination in bulks due to own weight taking into account the construction sequence. Proc. Inst. Struct. Mech. **57**(3), 529–536 (1953)
23. Brown, C.B., Green, D.R., Pawsey, S.: Flexible culverts under light fills. J. Struct. Div. ASCE **94**(4), 905–917 (1968)
24. Christion, P.P., Chuntranuluk, S.: Retaining wall under action of accreted tack fill. J. Geotech. Engry. Div. ASCE **100**(4), 471–476 (1974)
25. Brown, C.B., Evans, K.J., Lachapelle, E.R.: Slab avalanching and state of stress in fallen snow. J. Geophys. Res. **77**(24), 4570–4580 (1972)
26. Namov, V.E.: Mechanics of growing deformable solids—a review. J. Eng. Mech. (2), 207–210 (1994)
27. Shamina, V.A.: Formulation of the linear axisymmetric problem for deformable solids in terms of stresses, Vestnik Sankt-peterburgskogo Universiteta. Ser 1. Matematika Mekhanika Astronomiya **1**, 145–148 (2001)
28. Georgiyevskii, D.V., Pobedrya, B.Y.: The number of independent compatibility equations in the mechanics of deformable solids. J. Appl. Math. Mech. **68**(6), 941–946 (2004)
29. Cao, Z.Y.: Viscoelastic solution of time-varying solid mechanics. Acta Mech. Sin. **32**(4), 497–501 (2000)
30. Liang, G.: The viscoelastic time-varying analytical solutions of up-growing rectangular plane considering the gravity. J. Shanghai Maritime Univ. **21**(4), 73–79 (2000)
31. Wang, H.N., Cao, Z.Y.: Time-varying analytics study of random expanding hole in plane viscoelasticity. Acta Mech. Solida Sin. **27**(3), 319–323 (2006)